

1.1 Introduction

Textile structures are known for their unique combination of light weight and flexibility and their ability to offer a combination of strength and toughness. Textile structures have long been recognized as an attractive reinforcement form for applications ranging from aircraft wings produced by Boeing Aircraft Co. in the 1920s to carbon-carbon nose cones produced by General Electric in the 1950s. Textile preforms are fibrous assemblies with prearranged fiber orientation preshaped and often preimpregnated with matrix for composite formation. The microstructural organization of fibers within a preform, or fiber architecture, determines the pore geometry, pore distribution and tortuosity of the fiber paths within a composite. Textile preforms not only play a key role in translating fiber properties to composite performance but also influence the ease or difficulty in matrix infiltration and consolidation. Textile preforms are the structural backbone for the toughening and net shape manufacturing of composites.

When combined with high-performance fibers, matrices and properly tailored fiber/matrix interfaces, the creative use of fiber architecture promises to expand the design options for strong and tough structural composites.

Of the large family of textile structures, 3-D fabrics have attracted the most serious interest in the aerospace industry and served as a catalyst in stimulating the revival of interest in textile composites. 3-D fabrics for structural composites are fully integrated continuous fiber assemblies having multiaxial in-plane and out-of-plane fiber orientation. More specifically, a 3-D fabric is one that is fabricated by a textile process, resulting in three or more yarn diameters in the thickness direction with fibers oriented in three orthogonal planes. The engineering application of 3-D composite has its origin in aerospace carbon-carbon composites. 3-D fabrics for composites date back to the 1960s, responding to the needs in the emerging aerospace industry for parts and structures that were capable of

withstanding multidirectional mechanical stresses and thermal stresses. Since most of these early applications were for high-temperature and ablative environments, carbon-carbon composites were the principal materials. As indicated in a review article by McAllister and Lachman [1], the early carbon-carbon composites were reinforced by biaxial (2-D) fabrics. Beginning in the early 1960s, it took almost a whole decade and the trial of numerous reinforcement concepts, including needled felts, pile fabrics and stitched fabrics, to recognize the necessity of 3-D fabric reinforcements to address the problem of poor interlaminar strength in carbon-carbon composites [2-4]. Although the performance of a composite depends a great deal on the type of matrix and the nature of the fiber-matrix interface, it appears that much can be learned from the experience of the role of fiber architecture in the processing and performance of carbon-carbon composites.

The expansion of global interest in recent years in 3-D fabrics for resin, metal and ceramic matrix composites is a direct result of the current trend in the expansion of the use of composites from secondary to primary load-bearing applications in automobiles, building infrastructures, surgical implants, aircraft and space structures. This requires a substantial improvement in the through-the-thickness strength, damage tolerance and reliability of composites. In addition, it is also desirable to reduce the cost and broaden the usage of composites from aerospace to automotive applications. This calls for the development of a capability for quantity production and the direct formation of structural shapes. In order to improve the damage tolerance of composites, a high level of through-thickness and interlaminar strength is required. The reliability of a composite depends on the uniform distribution of the materials and consistency of interfacial properties. The structural integrity and handleability of the reinforcing material for the composite is critical for large-scale, automated production. A method for the direct formation of the structural shapes would therefore greatly simplify the laborious hand lay-up composite formation process. With the experience gained in the 3-D carbon-carbon composites and the recent progress in fiber technology and computer-aided textile design and liquid molding technology, the class of 3-D fabric structures is increasingly being recognized as serious candidates for structural composites.

The importance of 3-D fabric reinforced composites in the family of textile structural composites is reflected in several recent books on the subject [5,6]. This chapter is intended to provide an introduction to 3-D textile reinforcements for composites. The discussion will focus on the pre-forming process and structural geometry of the four basic classes of integrated fiber architecture: woven, knit and braid, and orthogonal non-woven 3-D structure.

Table 1.1. Fiber architecture for composites

Level	Reinforcement system	Textile construction	Fiber length	Fiber orientation	Fiber entanglement
I	Discrete	Chopped fiber	Discontinuous	Uncontrolled	None
II	Linear	Filament yarn	Continuous	Linear	None
III	Laminar	Simple fabric	Continuous	Planar	Planar
IV	Integrated	Advanced fabric	Continuous	3-D	3-D

1.2 Classification of textile preforms

There is a large family of textile preforming methods suitable for composite manufacturing [7]. The key criteria for the selection of textile preforms for structural composites are (a) the capability for in-plane multiaxial reinforcement, (b) through-thickness reinforcement and (c) the capability for formed shape and/or net shape manufacturing. Depending on the processing and end use requirements some or all of these features are required.

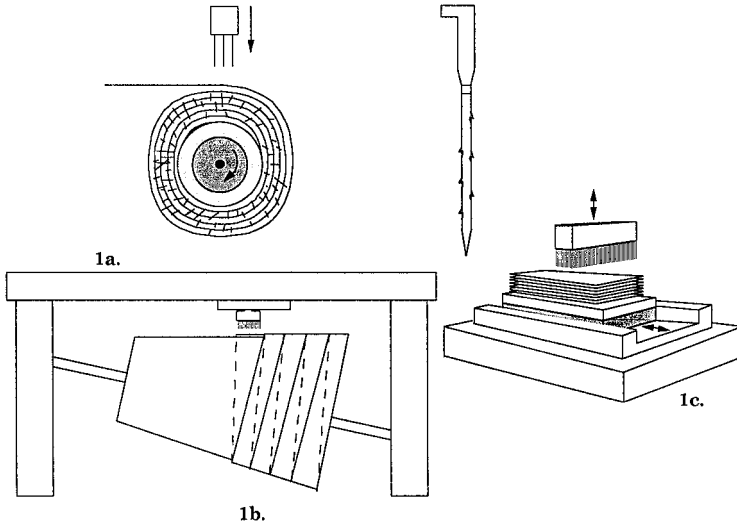
On the basis of structural integrity and fiber linearity and continuity, fiber architecture can be classified into four categories: discrete, continuous, planar interlaced (2-D) and fully integrated (3-D) structures. In Table 1.1 the nature of the various levels of fiber architecture is summarized [8].

A discrete fiber system such as a whisker or fiber mat has no material continuity; the orientation of the fibers is difficult to control precisely, although some aligned discrete fiber systems have recently been introduced. The structural integrity of the fibrous preform is derived mainly from interfiber friction. The strength translation efficiency, or the fraction of fiber strength translated to the non-aligned fibrous assembly of the reinforcement system, is quite low.

The second category of fiber architecture is the continuous filament, or unidirectional (0°) system. This architecture has the highest level of fiber continuity and linearity, and consequently has the highest level of property translation efficiency and is very suitable for filament wound and angle ply tape lay-up structures. The drawback of this fiber architecture is its intra- and interlaminar weakness owing to the lack of in-plane and out-of-plane yarn interlacings.

A third category of fiber reinforcement is the planar interlaced and inter-looped system. Although the intralaminar failure problem associated with the continuous filament system is addressed with this fiber architecture, the interlaminar strength is limited by the matrix strength owing to the lack of through-thickness fiber reinforcement.

The fully integrated system forms the fourth category of fiber architecture wherein the fibers are oriented in various in-plane and out-of-plane



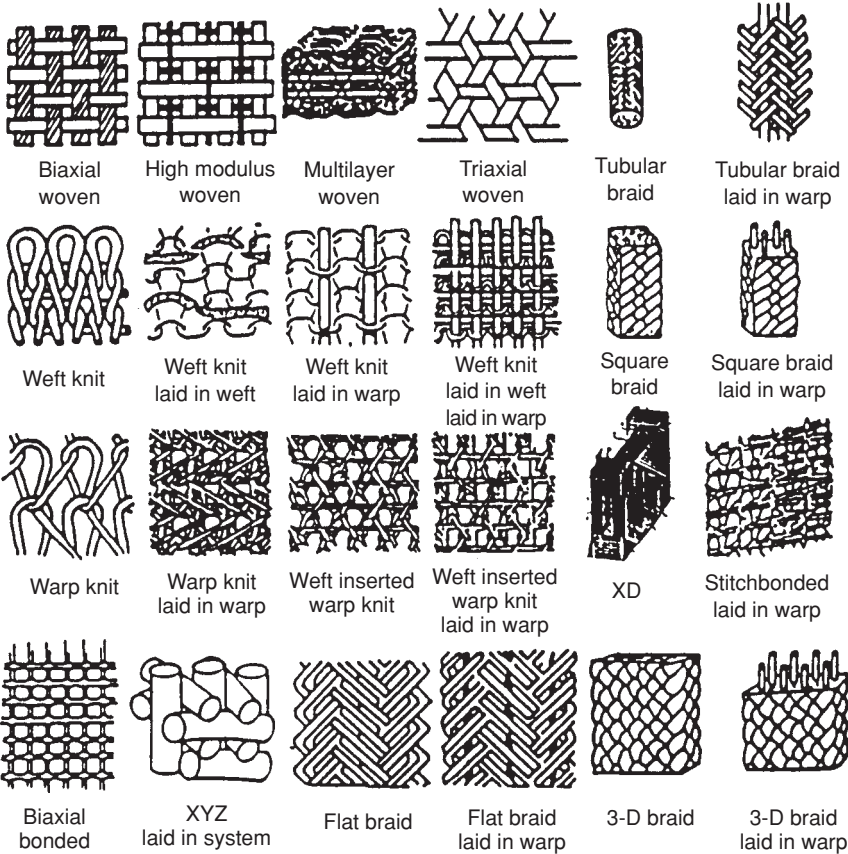
1.1 The Noveltex® method.

directions. With the continuous filament yarn, a 3-D network of yarn bundles is formed in an integral manner. The most attractive feature of the integrated structure is the additional reinforcement in the through-thickness direction which makes the composite virtually delamination-free. Another interesting aspect of many of the fully integrated structures such as 3-D woven, knits, braids and non-wovens is their ability to assume complex structural shapes.

Another way of classifying textile preforms is based on the fabric formation techniques. The conversion of fiber to preform can be accomplished via the 'fiber to fabric' (FTF) process, the 'yarn to fabric' (YTF) process and combinations of the two. An example of the FTF process is the Noveltex® method developed by P. Olry at SEP (Société Européenne de Propulsion, Bordeaux, France) [9]. As shown in Fig. 1.1, the Noveltex concept is based on the entanglement of fiber webs by needle punching. A similar process is being developed in Japan by Fukuta [10] using fluid jets in place of the needles to create through-thickness fiber entanglement.

The YTF processes are popular means for preform fabrication wherein the linear fiber assemblies (continuous filament) or twisted short fiber (staple) assemblies are interlaced, interlooped or intertwined to form 2-D or 3-D fabrics. Examples of preforms created by the YTF processes are shown in Fig. 1.2. A comparison of the basic YTF processes is given in Table 1.2.

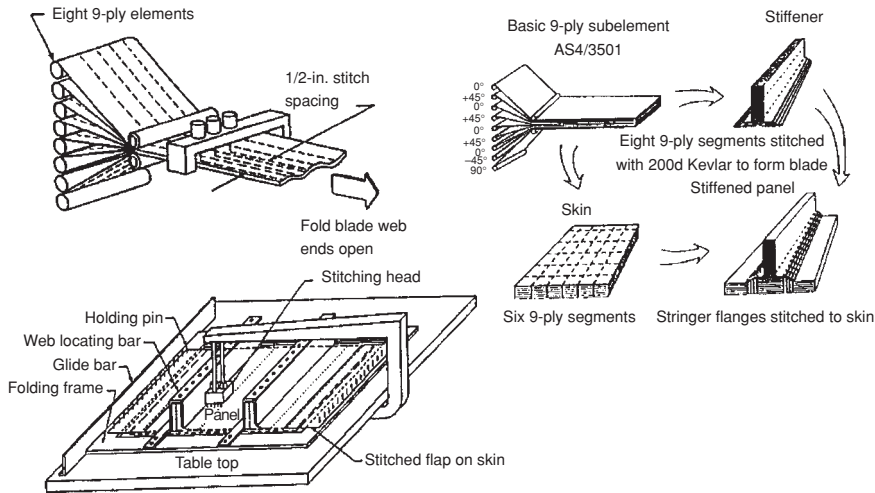
In addition to the FTF and YTF processes, textile preforms can be fabricated by combining structure and process. For example, the FTF webs



1.2 Examples of yarn-to-fabric preforms.

Table 1.2. A comparison of yarn-to-fabric formation techniques

YTF processes	Basic direction of yarn introduction	Basic formation technique
Weaving	Two (0°/90°)	Interlacing (by selective warp and fill insertion of 90° yarns into 0° yarn system)
Braiding	One (machine direction)	Intertwining (position displacement)
Knitting	One (0° or 90°)	Interlooping (by drawing warp or fill loops of yarns over previous loops)
Nonwoven	Three or more (orthogonal)	Mutual fiber placement

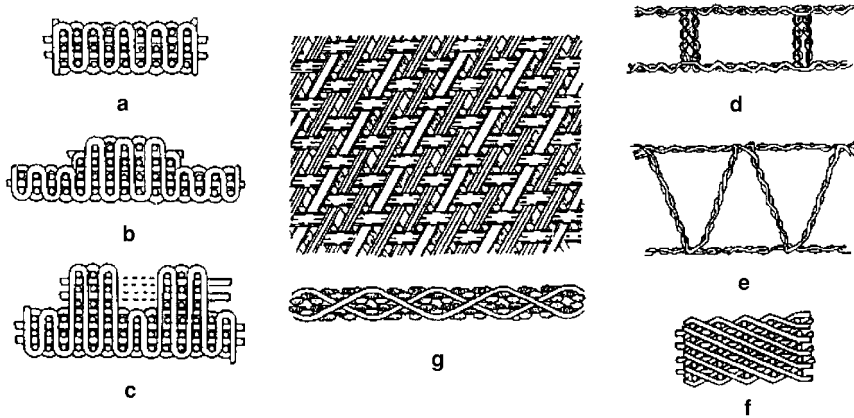


1.3 Combination of FTF and YTF processes.

can be incorporated into a YTF preform by needle or fluid jet entanglement to provide through-the-thickness reinforcement. Sewing is another example that can combine or strategically join FTF and/or YTF fabrics together to create a preform having multidirectional fiber reinforcement [11] (Fig. 1.3).

1.3 Structural geometry of 3-D textiles

The structural geometry of 3-D textiles can be characterized at both the macroscopic and the microscopic levels. At the macroscopic level, the external shape and the internal cellular structures are the result of a particular textile process and fabric construction employed in the creation of the structure. Similar shape and cellular geometry may be created by different textile processes. For example, a net shape I-beam can be produced by a weaving, braiding or knitting process. However, the microstructure or the fiber architecture produced by these three processes are quite different. This will lead to different levels of translation efficiency of the inherent fiber properties to the composite as well as different levels of damage-resistant characteristics. The efficient translation of fiber properties to the composite depends on the judicious selection of fiber architecture which is governed by the directional concentration of fibers. This directional fiber concentration can be quantified by fiber volume fraction V_f and fiber orientation, θ . Depending upon the textile manufacturing process used and the type of fabric construction, families of $V_f - \theta$ functions can be generated. These $V_f - \theta$ functions can be developed by geometrical modeling as



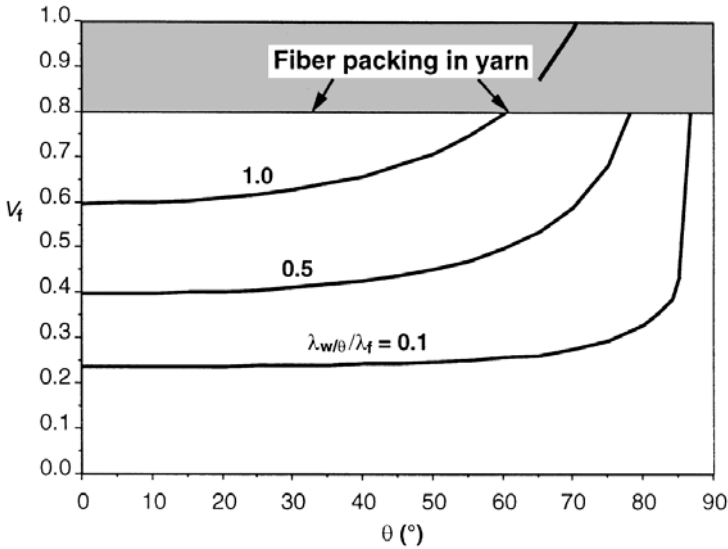
1.4 3-D woven fabrics.

detailed by Ko and Du [12]. Accordingly, the structure–property relationship of 3-D textile composites is a result of the dynamic interaction of microstructural and macrostructural geometries. In this section, the structural shapes, cellular structures and fiber architectures expressed in terms of the $V_f - \theta$ functions are presented for the four basic classes of 3-D textile reinforcements.

1.3.1 3-D woven fabrics

3-D woven fabrics are produced principally by the multiple-warp weaving method which has long been used for the manufacturing of double and triple cloths for bags, webbings and carpets. By the weaving method, various fiber architectures can be produced including solid orthogonal panels (Fig. 1.4a), variable thickness solid panels (Fig. 1.4b, c), and core structures simulating a box beam (Fig. 1.4d) or a truss-like structure (Fig. 1.4e). Furthermore, by proper manipulation of the warp yarns, as exemplified by the angle interlock structure (Fig. 1.4f), the through-thickness yarns can be organized into a diagonal pattern. To address the inherent lack of in-plane reinforcement in the bias direction, Dow [13] modified the triaxial weaving technology to produce multilayer triaxial fabrics as shown in Fig. 1.4(g).

Through unit cell geometric modeling the $V_f - \theta$ functions can be generated for various woven fabrics. Figure 1.5 plots total fiber volume fraction versus web interlock angle for an angle interlock 3-D woven fabric, with three levels of linear density ratio. For purposes of calculation, the fiber packing fraction is assumed to be 0.8, which provides the upper limit for possible fiber volume fraction. The fabric tightness factor (η) used is 0.2.



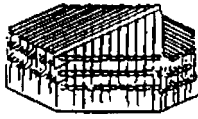
1.5 Process window of fiber volume fraction for 3-D woven ($\lambda_{w/\theta}$ is linear density of warp or web yarn, λ_f is linear density of filled yarn).

1.3.2 Orthogonal non-woven fabrics

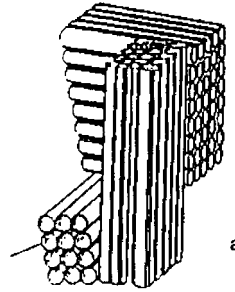
Pioneered by aerospace companies such as General Electric [14], the non-woven 3-D fabric technology was developed further by Fiber Materials Incorporated [15]. Recent progress in automation of the non-woven 3-D fabric manufacturing process was made in France by Aérospatiale [16], SEP [9] and Brochier [17,18] and in Japan by Fukuta and Coworkers [19,20].

The structural geometries resulting from the various processing techniques are shown in Fig. 1.6. Figure 1.6(a) and (b) show the single bundle XYZ fabrics in a rectangular and cylindrical shape. In Fig. 1.6(b), the multidirectional reinforcement in the plane of the 3-D structure is shown. Although most of the orthogonal non-woven 3-D structures consist of linear yarn reinforcements in all of the directions, introduction of the planar yarns in a non-linear manner, as shown in Fig. 1.6(c), (d) and (e) can result in an open lattice or a flexible and conformable structure.

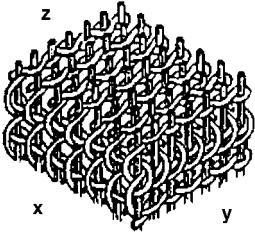
Based on the unit cell geometry shown in Fig. 1.7, assuming an orthogonal placement of yarns in all three directions, the $V_f - \theta$ function was constructed for an orthogonal woven fabric. Figure 1.8 plots the fiber volume fraction versus d_y/d_x (fiber diameter) ratios, assuming a fiber packing fraction of 0.8. For all three levels of d_z/d_x ratios, the fiber volume fraction first decreases with the increase in d_y/d_x ratio, reaches a minimum, and then increases. As can be seen in the figure, the maximum fiber volume fraction is about 0.63 at either high or low d_y/d_x ratios, whereas the minimum fiber



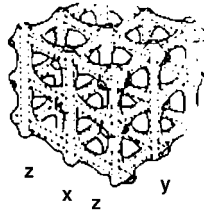
b



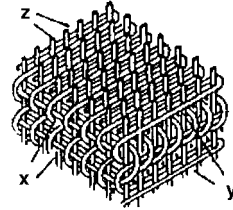
a



c

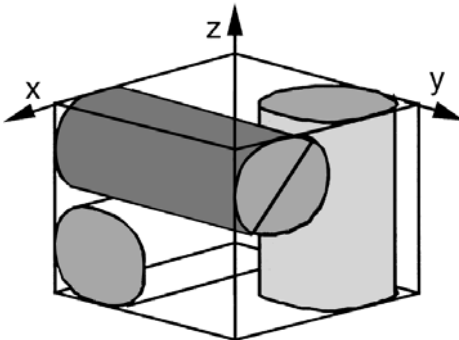


e



d

1.6 Orthogonal woven fabrics.



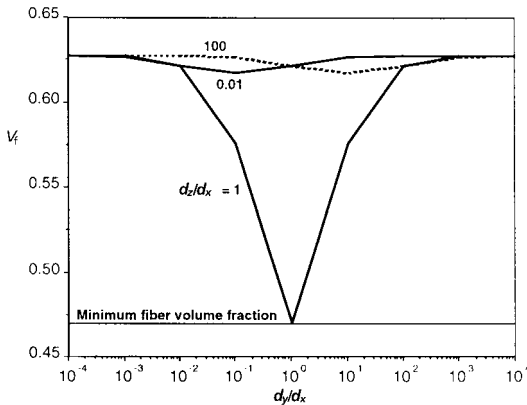
1.7 Unit cell for orthogonal non-woven fabrics.

volume fraction of about 0.47 is achieved when both d_y/d_x and d_z/d_x ratios are equal to 1.

1.3.3 Knitted 3-D fabrics

The knitted 3-D fabrics are produced by either the weft knitting or warp knitting process. An example of a weft knit is the near net shape structure

Copyrighted Material downloaded from Woodhead Publishing Online
 Delivered by http://woodhead.metapress.com
 Hong Kong Polytechnic University (714-57-975)
 Saturday, January 22, 2011 12:29:37 AM
 IP Address: 158.132.122.9

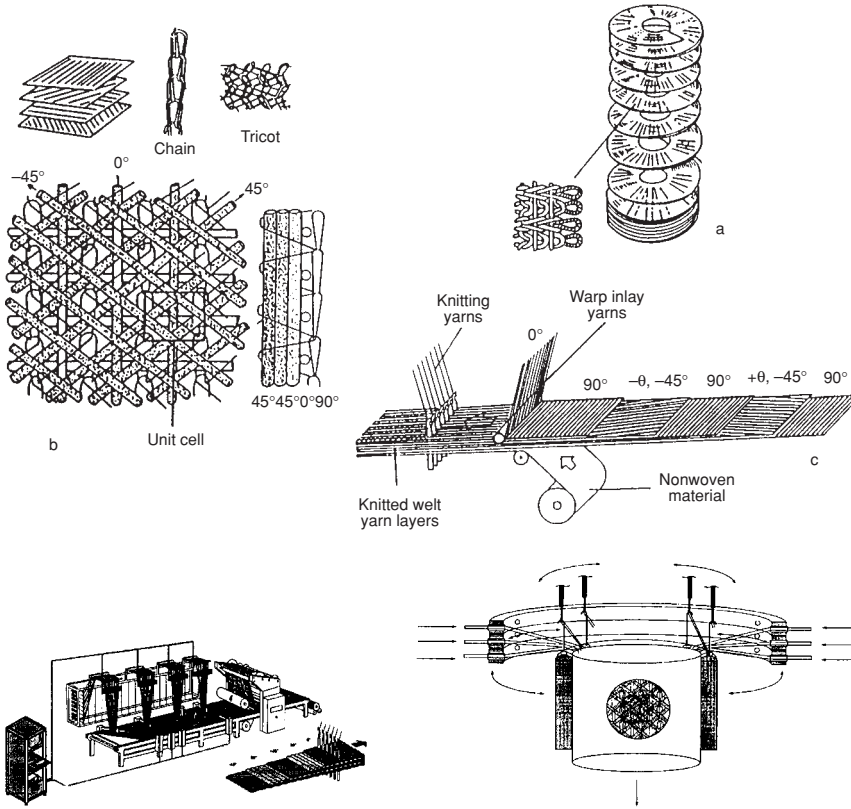


1.8 Process window of fiber volume fraction for orthogonal non-woven fabrics.

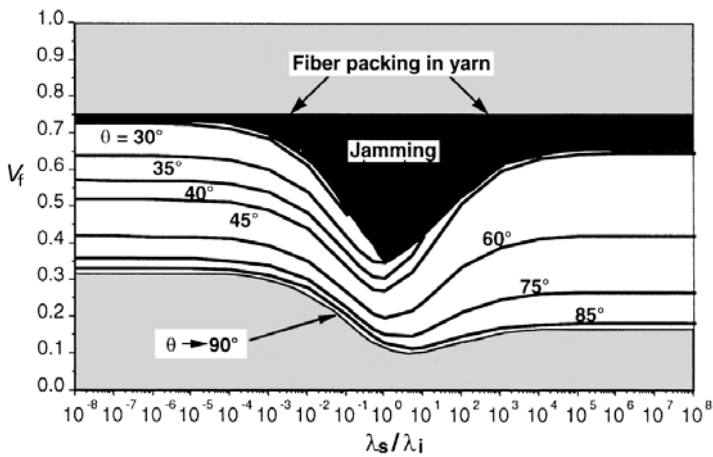
knitted by the Pressure Foot® process [21] (Fig. 1.9a). In a collapsed form this preform has been used for carbon-carbon aircraft brakes. The unique feature of the weft knit structures is their conformability [22]. By strategic introduction of linear reinforcement yarns, weft knitted structures can be used effectively for forming very complex shape structures. While the suitability of weft knit for structural applications is still being evaluated, much progress has been made in the multiaxial warp knit (MWK) technology in recent years [23,24]. From the structural geometry point of view, the MWK fabric systems consist of warp (0°), weft (90°) and bias ($\pm\theta$) yarns held together by a chain or tricot stitch through the thickness of the fabric, as illustrated in Fig. 1.10(b). The logical extension of the MWK technology is the formation of circular multiaxial structures by the warp knitting process. This technology (Fig. 1.9d) has been demonstrated in the Institute of Textiles of the University of Aachen [25].

An example of MWK is the LIBA system, as shown in Fig. 1.9(c) and (d). Six layers of linear yarns can be assembled in various stacking sequences along with a fiber mat and can be integrated together by knitting needles piercing through the yarn layers.

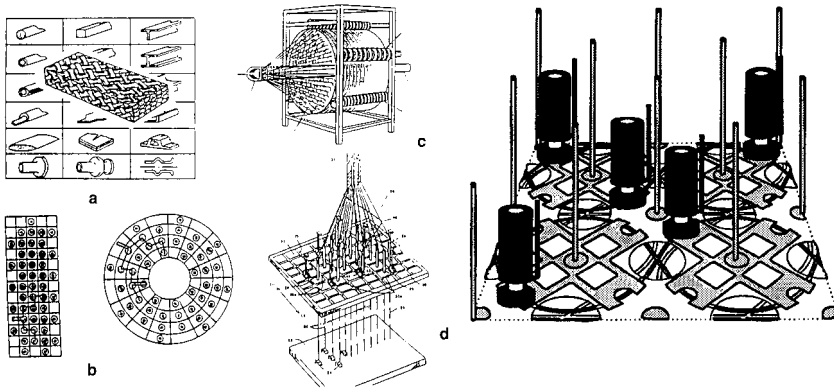
The unit cell geometric analysis of a four-layer system is used as an example to generate the $V_f - \theta$ functions for the MWK fabric [26]. This analysis can be generalized to include other MWK systems with six or more layers of insertion yarns. The fiber volume fraction relation in Fig. 1.10 shows that for the fixed parameters selected, only a limited window exists for the MWK fabric construction. The window is bounded by two factors: yarn jamming and the point of 90° bias yarn angle. Fabric constructions corresponding to the curve marked 'jamming' are at their tightest allowable point, and constructions at the $\theta \rightarrow 90^\circ$ curve have the most open structure.



1.9 3-D knitted fabrics.



1.10 Fiber volume fraction versus ratio of stitch-to-insertion yarn linear density (tricot stitch, $\kappa = 0.75$, $\rho = 2.5 \text{ kg/m}^3$, $f_i = 5$ and $\eta = 0.5$).



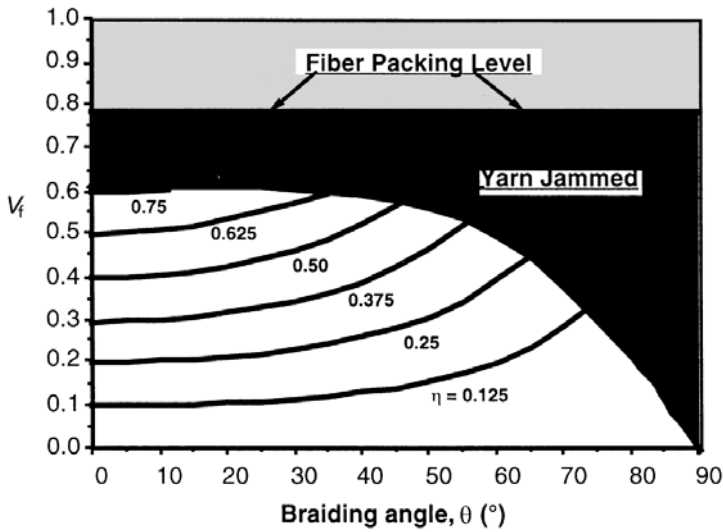
1.11 3-D braided fabrics.

When $\theta < 30^\circ$, jamming occurs in the whole range of yarn linear density ratio from zero to infinity. When θ is in the range of 30° to 40° , the fiber volume fraction decreases with an increase in yarn linear density ratio until jamming occurs. When $\theta = 45^\circ$, the fiber volume fraction decreases with an increase in yarn linear density ratio to a minimum at about $\lambda_s/\lambda_i = 1$, and starts to increase until jamming occurs (λ_s = stitch yarn diameter, λ_i = insert yarn diameter). When $\theta \geq 60^\circ$, the fiber volume fraction has the same trend as when $\theta = 45^\circ$, but yarn jamming never occurs. The fiber packing in the yarns, taken as 0.75, limits the maximum fiber volume fraction in the fabric.

1.3.4 3-D braided fabrics

3-D braiding technology is an extension of the well-established 2-D braiding technology wherein the fabric is constructed by the intertwining of two or more yarn systems to form an integral structure. 3-D braiding is one of the textile processes wherein a wide variety of solid complex structural shapes (Fig. 1.11a) can be produced in an integral manner, resulting in a highly damage-resistant structure. Figure 1.11(b) shows two basic loom set-ups in circular and rectangular configurations [27]. The 3-D braids are produced by a number of processes including the track and column method [28] (Fig. 1.11c), the two-step method [29] (Fig. 1.11d) as well as a variety of displacement braiding techniques by discrete or continuous motions [30]. The basic braiding motion includes the alternate X and Y displacement of yarn carriers followed by a compacting motion. The formation of shapes is accomplished by the proper positioning of the carriers and the joining of various rectangular groups through selected carrier movements.

Based on unit cell geometry analysis, Fig. 1.12 shows the $V_f - \theta$ relationship prior to and at the jamming condition [31]. The fiber packing fraction,



1.12 Relationship of fiber volume fraction to braiding angle for various tightness factors [31].

κ , is assumed as 0.785. As can be seen, there are three regions of fiber volume fraction. The upper region cannot be achieved owing to the impossible fiber packing in a yarn bundle. Jamming occurs when the highest braiding angle is reached for a given fabric tightness factor η . The non-shaded region is the working window for a variety of $V_f - \theta$ combinations. Clearly, for a given fabric tightness, the higher braiding angle gives a higher fiber volume fraction and, for a fixed braiding angle, the fiber volume fraction is greater at higher tightness factors.

1.4 Tailoring fiber architecture for strong and tough composites

Strength and toughness are usually considered to be concomitant mechanical properties for traditional engineering materials. By properly manipulating fiber architecture, the degree of freedom permitted in the engineering of strong and tough composite materials is greatly increased.

The strengthening effect of fiber on polymer matrix composites is well established. The role of fiber in the toughening of ceramic matrix composites is now generally recognized. A major challenge in advanced composite materials is to achieve a balance of strengthening and toughening effects. While well-oriented linear unitape composites provide the maximum strengthening effect when loading is along the fiber direction, the interlaced non-linear integrated systems tend to maximize damage containment and

enhance toughness. Expanding from these strengthening and toughening concepts, one may hypothesize that a combination of the strategically placed linear fibers in a 3-D integrated fiber network would provide the necessary ingredients for a strong and tough composite. The linear fibers and the fibers that make up the 3-D fiber network can be from the same material family but differ in diameter or bundle size. Alternatively, the two material systems can be quite different, each contributing unique properties such as strength, stiffness and thermal stability to the composite structure. To demonstrate this geometric/material hybrid concept, let us examine three examples, polymer matrix composites (PMC), metal matrix composites (MMC) and ceramic matrix composites (CMC), wherein different proportions of linear fibers were placed in a 3-D braided fiber network.

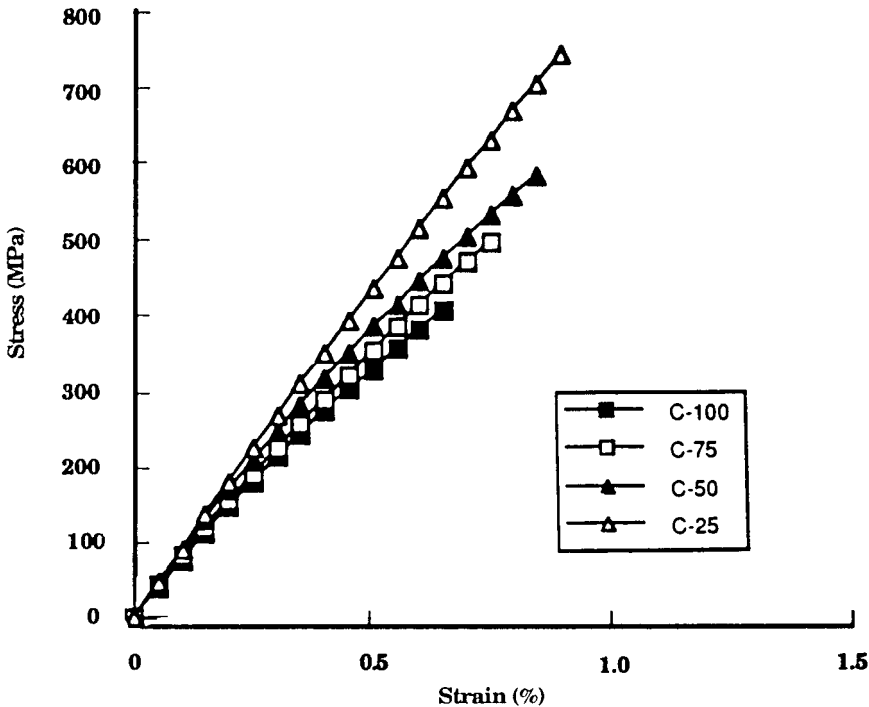
1.4.1 Polymer matrix composites

The hybrid concept has been demonstrated in several previous studies for PMC. For example, it was found that a combination of linear fibers in a 3-D braided structure improves the compression-after-impact strength of PEEK/carbon composites [32]. It was further demonstrated that the linear fibers provide additional flexibility in modifying the failure modes of the composites whereas the 3-D fiber network greatly reduces the damage area caused by impact loading.

In a controlled study [33], the compressive stress–strain behavior of carbon, glass and Kevlar fibers in an Epon 828/DETA matrix with linear fiber to 3-D braided fiber ratio ranging from 0/100 to 75/25 was examined. It was found that, in all three cases, both the compressive strength and the elongation to break increase as the proportion of linear fibers increases. This strengthening and toughening effect is illustrated in Fig. 1.13, which shows that the compressive strength of the carbon/epoxy composites increases from 415 MPa to 760 MPa as the proportion of linear fibers in the 3-D braided structure increases from 0/100 to 75/25. Likewise, elongation to breaking increases from 0.7% to 0.9%.

1.4.2 Metal matrix composites

The concepts of geometric and material hybrids for MMC are demonstrated using a combination of SCS-6 SiC filaments in a 3-D braided Nicalon SiC reinforced Al 6061 composite [34]. The hybrid effect was studied by tensile, notched beam three-point bending and compact tension tests of the 3-D braided composites. The hybrid braided SiC/AL-6061 composites studied include a 0/100, 25/75, 50/50 and 75/25 combination of linear SCS with 3-D braided Nicalon. Addition of the strong and stiff SCS filaments to the Nicalon reinforced aluminum strengthens the composites and



1.13 Compressive stress–strain behavior of carbon/epoxy composites.

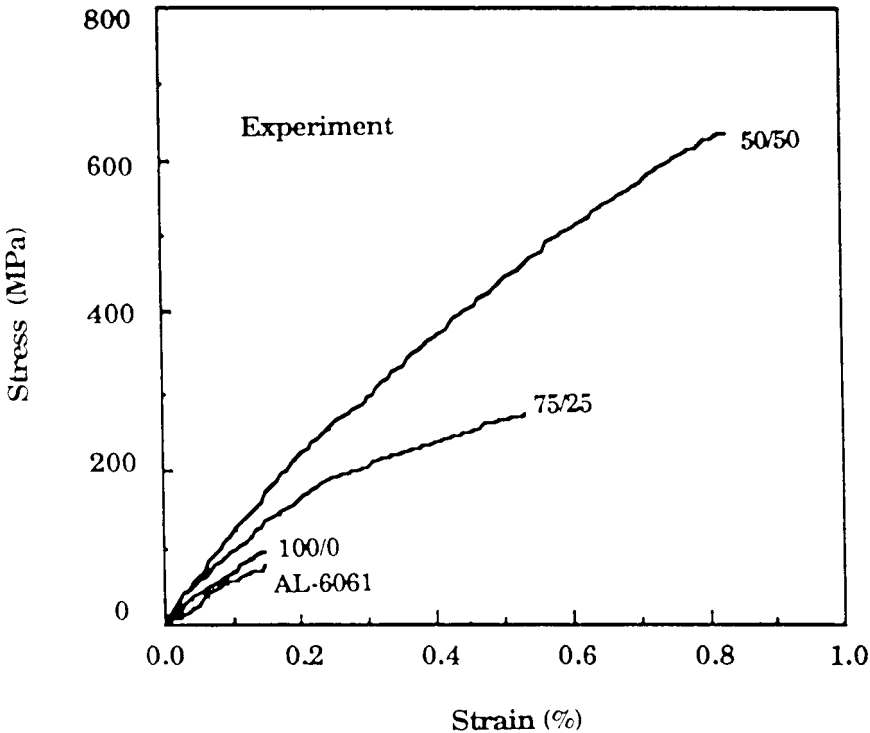
modifies the composite failure mode from matrix-dominated failure to linear yarns controlled failure.

Figure 1.14 shows the stress–strain curves of the MMC reflecting the non-linear behavior of the composites. In comparison to the pure cast aluminum sample, the 100% braided composites show only a slight reinforcement effect whereas the hybrid composites show a remarkable improvement in strength (121 to 599 MPa) and toughness (0.15% to 0.81% failure strain) as the percentage of longitudinal SCS-6 lay-in yarns increases from 0 to 50%.

The effect of geometric and material hybrids on the fracture behavior can be illustrated using the response of the MMC to 3-point bending tests. As shown in Fig. 1.15, the onset fracture load increases as the percentage of SCS-6 filaments increases. When the propagating crack reaches a bundle of SCS-6 filaments, the crack propagation rate is delayed and gradual failure occurs, as illustrated in the zig-zag pattern of the load–deflection curves.

1.4.3 Ceramic matrix composites

Employing the same material–geometric hybrid system used in the MMC study, various proportions (ranging from 0/100, 25/75, 50/50 to 75/25) of

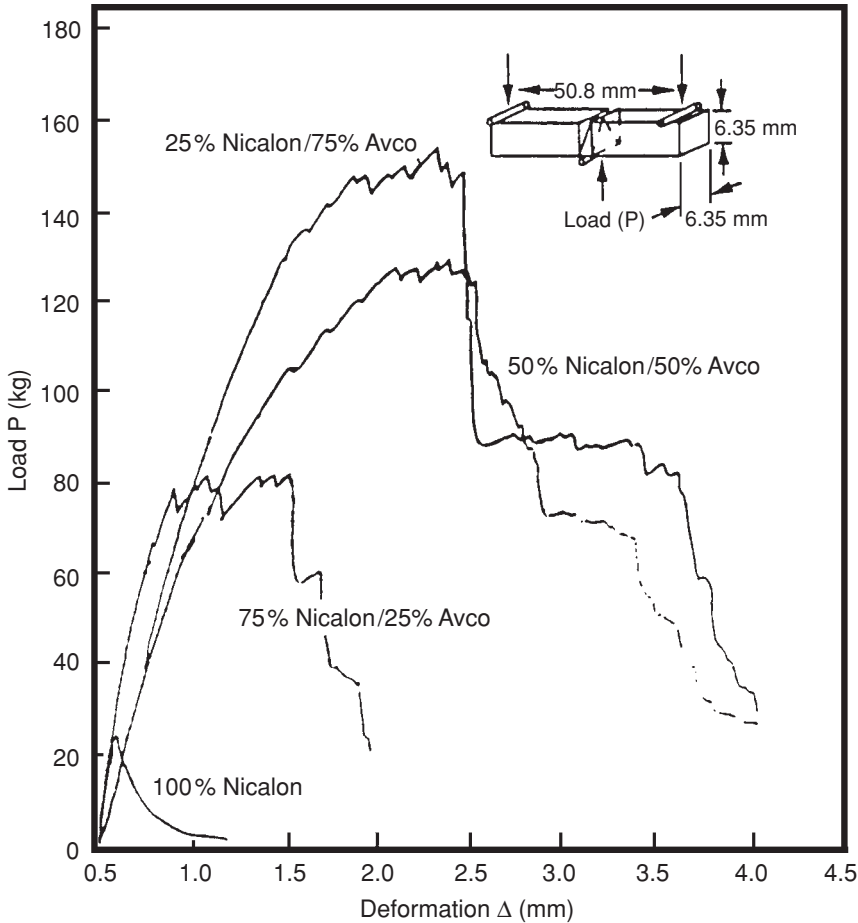


1.14 Tensile stress-strain behavior of 3-D braided SiC/Al composites.

SCS-6/Nicalon 3-D braid were fabricated in a lithium aluminum silicate (LAS III) matrix. Tensile, flexural and fracture tests were carried out on the 3-D braided CMC [35]. Besides enhancing strength, the thermally stable SCS filament played a significant role in preserving the structural integrity of the composite during processing and under high-temperature oxidation end-use environments. By placing the strong and stiff SCS filaments in the axial (0°) direction in the 3-D braided Nicalon fiber network, a significant improvement in tensile strength as well as the first cracking strength were achieved in the SiC/SiC/LAS III structure (Fig. 1.16). It is remarkable to observe that the elongation to break of the hybrid composites also increases with the increase of the proportion of SCS filaments, resulting in a much strengthened and toughened CMC.

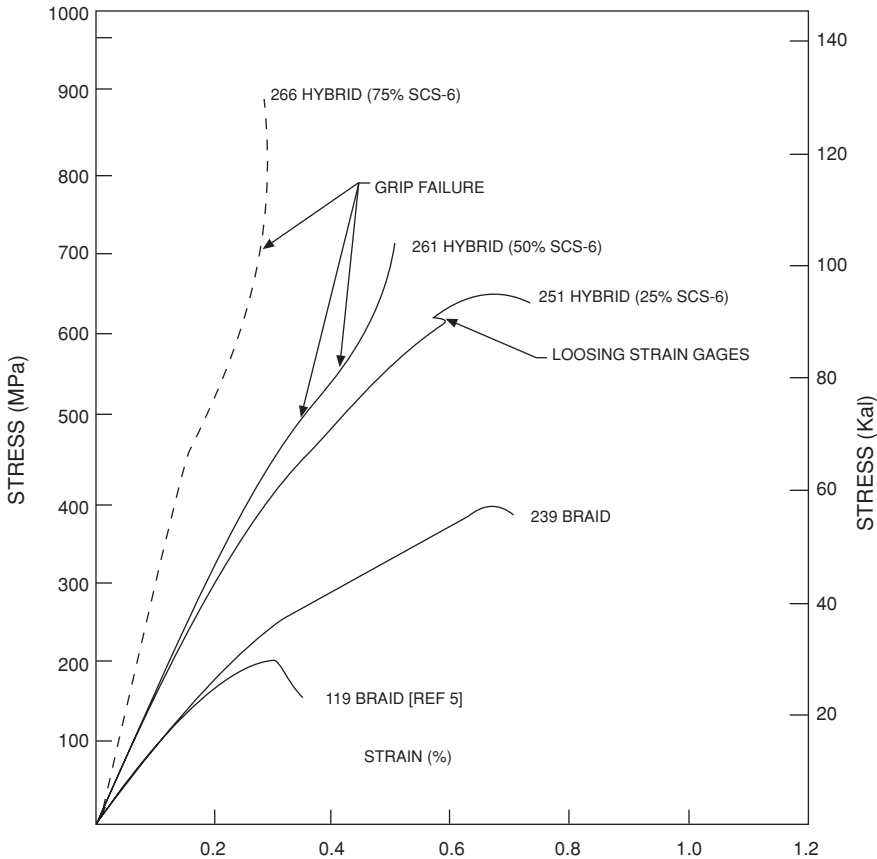
1.5 Modeling of 3-D textile composites

Given a large family of fiber architectures which can be generated by an impressive array of textile preforming techniques, it is quite evident that one can tailor composite properties to meet various end-use requirements.



1.15 Fracture behavior of 3-D braided SiC/Al composites by three-point bend test.

In order to facilitate the rational selection and to stimulate the creative design of fiber architecture by textile preforming, a science-based design framework must be established to bridge the communication gap between textile technologists, composite materials engineers and structural design engineers. This framework must be capable of relating preform manufacturing parameters to fiber architectural geometry as well as material properties. This design framework can be constructed through three levels of modeling including topological, geometrical and mechanical models. The topological model is a quantitative description of the preforming process. The geometrical model is the heart of the design framework which quantifies fiber orientation and fiber volume distribution in terms of fiber bundle



1.16 Tensile stress–strain behavior of 3-D braided SiC/LAS III composites.

(yarn) and fabric structural geometry created by the preforming process. The mechanical model provides the link between the mechanical properties of the material system and the fiber architecture. The product of the mechanical model is the stress–strain response of the textile reinforced composite for a given boundary condition as well as a stiffness matrix reflecting the material and fiber architecture contribution to the properties of the composite system. With the stiffness matrix, the structural designer can perform finite element analysis with meaningful information, thus facilitating the integration of material design concepts, manufacturing processes and structural design to product engineering.

The mechanical properties of textile reinforced composites can be predicted with a knowledge of the fiber properties, matrix properties and textile preform fiber architecture through a modified laminate theory

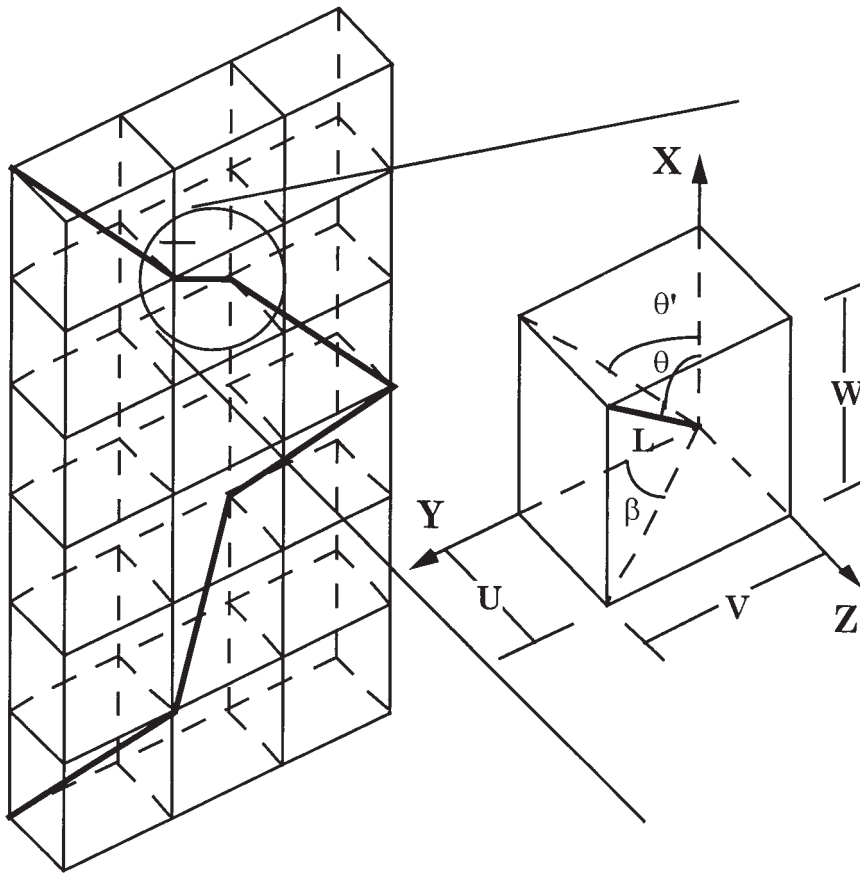
approach. Geometric unit cells defining the fabric structure (or textile preform) can be identified and quantified to form a basis for the analysis. For 2-D woven fabric reinforced composites, Dow [35] and Chou and Yang [36] have developed models for the thermomechanical properties of plain, twill and satin reinforced composites. Examples of these include the mosaic, crimp and bridging models developed by Chou. In the mosaic model, fiber continuity is ignored and the composite is treated as an assembly of cross-ply elements. With the crimp model, the non-linear crimp geometry as well as yarn continuity is considered. Based on the geometric repeating unit cell, each yarn segment is treated as laminar. While the crimp model was found to be most suitable for plane weave composites, the bridging model was found to be best for satin weave composites, as it takes the relative stiffness contribution of the linear and non-linear yarn segments into consideration. Over the past decade, as reviewed by Cox and Flanagan [38], an impressive number of models have been developed for textile composites.

The modeling of 3-D fiber reinforced composites begins with the establishment of geometric unit cells. Using 3-D braided composites as an example the following illustrates an approach which focuses on the integration of fiber architecture design for manufacturing. From a 'preform processing science' point of view, Pastore and Ko [39] developed a 'fabric geometry model' (FGM) based on the unit cell geometry shown in Fig. 1.12. The stiffness of a 3-D braided composite was considered to be the sum of stiffnesses of all its laminae. The unit cell for the 3-D braid can be represented by several yarns running parallel to the body diagonal of the cell. However, in some instances, yarns are placed in longitudinal (0°) and transverse (90°) directions of the fabric and are referred to as longitudinal and transverse reinforcements (or lay-ins) respectively. The preform processing parameters are specifically related to corresponding unit cell geometries. The geometric descriptions form the basis for an FGM which models a characteristic volume. Accordingly, the generation of the stiffness matrix through the FGM provides a link between microstructural design and macrostructural analysis.

In order to establish a geometric model and method for analyzing the properties of the 3-D braid, it is necessary first to identify the orientation of the yarns in the 3-D fiber network. Figure 1.17 shows a typical 3-D braided structure with an enlarged view of the unit cell. Processing parameters U , V and W , representing the thickness, width and height of the unit cell, are related by the following equation:

$$W = \frac{\sqrt{U^2 + V^2}}{\tan \theta} \quad [1.1]$$

where θ , the interior angle, defines the orientation of the yarn with respect to the longitudinal axis of the panel. Given this relationship, it is possible



1.17 Unit cell geometry for the fabric geometry model.

to identify the angle θ associated with a particular fabric system, or to determine the value of W necessary to manufacture a fabric with fiber orientation θ .

Once the interior angle θ has been identified for a given system, the relation between the desirable fiber volume fraction and the total number of yarns needed in the composite can be established as follows:

$$V_f = \frac{N_y D_y}{C_d A_c \rho \cos \theta} \tag{1.2}$$

where: N_y = total number of yarns in the fabric,

$C_d = 9 \times 10^5$, is a constant,

A_c = cross-sectional area of finished composite (cm^2),

ρ = density of fiber (g/cc),

θ = interior angle, defined in Equation 1,
 D_y = linear density of fiber (denier),
 V_f = fiber volume fraction.

Once the fabric geometry has been quantified, the result can be used together with the fiber and matrix properties to predict the mechanical properties of the composite system through a modified lamination theory. From the geometry of a unit cell associated with a particular fiber architecture, different systems of yarn can be identified whose fiber orientations are defined by their respective interior angle θ and azimuthal angle β , as previously shown in Fig. 1.17. Assuming each system of yarn can be represented by a comparable unidirectional lamina with an elastic stiffness matrix defined as follows:

$$[C] = \begin{pmatrix} c_{11} & c_{12} & c_{13} & 0 & 0 & 0 \\ & c_{22} & c_{23} & 0 & 0 & 0 \\ & & c_{33} & 0 & 0 & 0 \\ & & & c_{44} & 0 & 0 \\ & & & & c_{55} & 0 \\ & & & & & c_{66} \end{pmatrix} \quad [1.3]$$

where: $c_{11} = (1 - n_{23}^2)E_{11}/K^*$,
 $c_{22} = c_{33} = (1 - n_{12}n_{21})E_{22}/K^*$,
 $c_{12} = c_{13} = (1 + n_{23})n_{21}E_{11}/K^*$,
 $c_{23} = (n_{23} + n_{12}n_{21})E_{22}/K^*$,
 $c_{44} = G_{23}$,
 $c_{55} = G_{13}$,
 $c_{66} = G_{12}$,
 $K^* = 1 - 2n_{12}n_{21}(1 + n_{23}) - n_{23}^2$,

then the elastic stiffness matrix $[C']$ of this yarn system in the longitudinal direction of the panel can be expressed as

$$[C'] = [T][C][T]^{-1} \quad [1.4]$$

in which the transformation matrix

$$[T] = \begin{pmatrix} l_1^2 & m_1^2 & n_1^2 & 2m_1n_1 & 2l_1n_1 & 2l_1m_1 \\ l_2^2 & m_2^2 & n_2^2 & 2m_2n_2 & 2l_2n_2 & 2l_2m_2 \\ l_3^2 & m_3^2 & n_3^2 & 2m_3n_3 & 2l_3n_3 & 2l_3m_3 \\ l_2l_3 & m_2m_3 & n_2n_3 & m_2n_3 + m_3n_2 & l_2n_3 + l_3n_2 & l_2m_3 + l_3m_2 \\ l_1l_3 & m_1m_3 & n_1n_3 & m_1n_3 + m_3n_1 & l_1n_3 + l_3n_1 & l_1m_3 + l_3m_1 \\ l_2l_1 & m_2m_1 & n_2n_1 & m_1n_2 + m_2n_1 & l_1n_2 + l_2n_1 & l_1m_2 + l_2m_1 \end{pmatrix} \quad [1.5]$$

where

$$\begin{aligned} l_1 &= \cos \theta & m_1 &= 0 & n_1 &= -\sin \theta \\ l_2 &= \sin \theta \cos \beta & m_2 &= \sin \beta & n_2 &= \cos \theta \cos \beta \\ l_3 &= \sin \theta \sin \beta & m_3 &= -\cos \beta & n_3 &= \cos \theta \sin \beta \end{aligned}$$

It is noted that the material properties of a unidirectional lamina, E_{11} , E_{22} , G_{12} , \dots , can be obtained easily using the well-established micromechanical relationships.

1.6 Application of the FGM

1.6.1 Prediction of stress–strain relationships

In order to determine the stress–strain behavior of the fabric reinforced composites, it is necessary to utilize each of the yarn systems. A model for yarn system interaction has been chosen wherein the stiffness matrices for each system of yarns are superimposed proportionately according to contributing volume to determine the fabric reinforced composite system stiffness:

$$[C] = \sum_i k_i [C']_j \quad [1.6]$$

where: $[C]$ = total stiffness matrix,
 k_i = fractional volume of the i th system of yarns.

In order to account for the potentially non-linear behavior of the materials, the system stiffness matrix should be calculated anew at each strain level. Thus the stress–strain behavior of the composite can be expressed as

$$\Delta \sigma = [C]_s [\Delta \epsilon] \quad [1.7]$$

where: $\Delta \sigma$ = incremental stress vector (6×1),
 $\Delta \epsilon$ = incremental strain vector (6×1).

From this, the stress vector can be determined as

$$\sigma = \sigma + \Delta \sigma \quad [1.8]$$

where: σ = stress vector (6×1).

A failure point for the composite is determined for each system of yarns by a maximum strain energy criterion. If the strain energy on the fiber exceeds the maximum allowable, that system of yarns has failed. Mathematically, if the following expression is true, the system has failed:

$$U_{c,i} \geq U_m \quad [1.9]$$

where: $U_m = \left| V_f(\sigma_{fu}(\epsilon_{fu})/2) + (1 - V_f) \int_0^{\epsilon_{fu}} \sigma_{\mu}(\epsilon) \epsilon d\epsilon \right|$,

σ_{fu} = fiber ultimate strength,

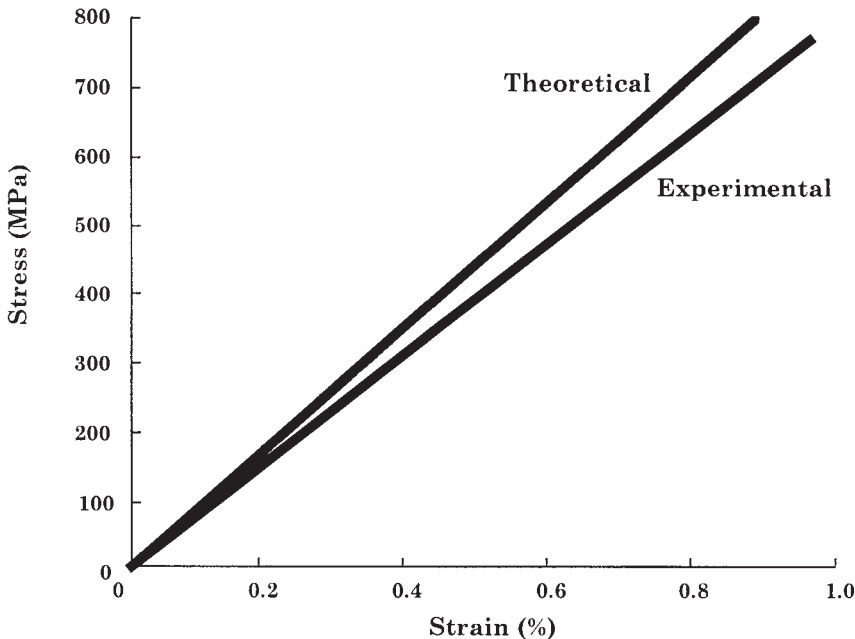
ϵ_{fu} = fiber ultimate strain,

U_{ci} = strain energy of the i th yarn system with strain ϵ_k ,

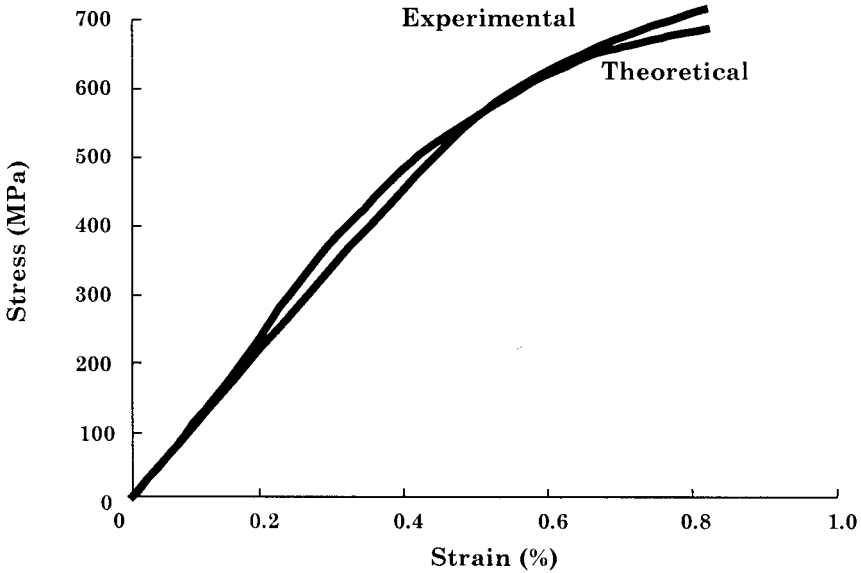
σ_{ci} = stress on the i th composite system.

Using these maximum energy criteria, a failure point for each system of yarns can be found. When a system of yarns fails, its contribution to the total system stiffness is removed. When all systems have failed, the composite is said to have failed. In this way, the entire stress–strain curve for the composite can be predicted up to the point of composite failure.

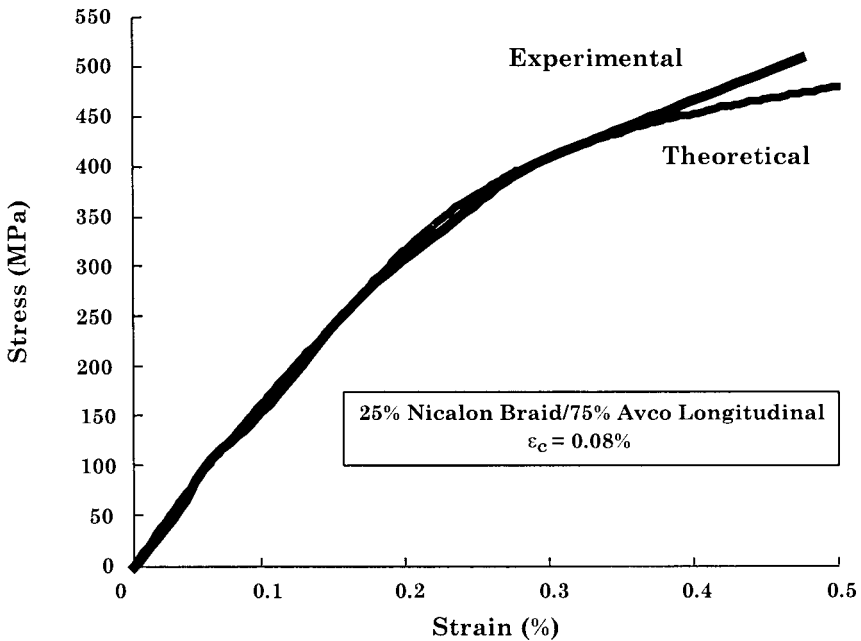
The FGM has been employed with satisfactory results to predict the stress–strain properties of polymer, metal and ceramic matrix components. Shown in Figs. 1.18, 1.19 and 1.20 are the theoretical and experimental tensile stress strain relatively of carbon/epoxy, SiC/Al and SiC/LAS III composites respectively.



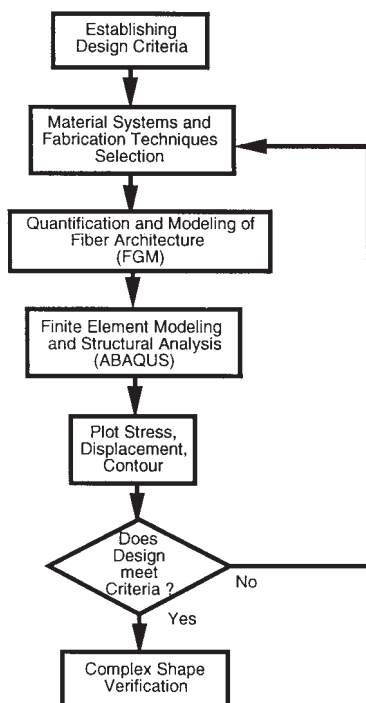
1.18 Theoretical and experimental compressive stress–strain relationship of 3-D braided carbon/epoxy composites.



1.19 Theoretical and experimental tensile stress-strain relationship of 3-D braided SiC/Al composites.



1.20 Theoretical and experimental tensile stress-strain relationship of 3-D braided SiC/LAS III composite.



1.21 An integrated design methodology for 3-D fabric composite structures.

1.6.2 Structural analysis of a 3-D braided composite turbine blade

By using the FGM analysis, one can obtain the elasticity matrix $[C]$ of a braided composite. In a displacement-based finite element formulation the stiffness matrix $[K]$ can be obtained from the equation

$$K = \int BTCB dy \quad [1.10]$$

where $[B]$ is the strain-displacement transformation matrix. Therefore, the FGM can be incorporated into general finite element analysis programs for solving braided composite structures with complex shapes. Data input to this program include fiber/matrix properties and braiding parameters, i.e. surface angle, inclined angle, fiber volume fraction and braiding percentage.

For illustration purposes, the integrated design for manufacturing methodology has been applied to the design and analysis of various complex-shape engine components. A brief outline of the procedure for the design of a composite turbine blade is shown in Fig. 1.21.

For a more detailed description and solution to the problem, readers are referred to reference [40]. In the design of the composite turbine blade, it has been established that the structure must be able to survive a certain

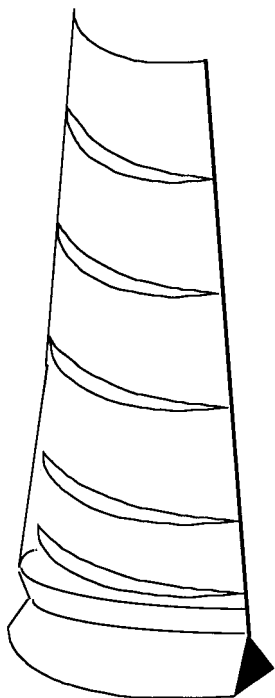
level of centrifugal force due to a given level of rotational speed and the thermal loading due to heated gas flow from the combustion chamber. In order to assess the fatigue life of the turbine blade, the natural frequencies of the blade must also be known. On the other hand, the aerodynamic analysis of a turbine rotor may impose certain restrictions on the thickness of blades, and the fiber architecture used may have to provide the structure with enough fiber volume fraction in some critical areas and directions. The selection of material systems and fabrication techniques will greatly influence the mechanical properties of the composite system and the responses of structural components, and is therefore the most important step in this design framework.

For each material system and fabrication technique selected as a possible candidate, the corresponding fiber architecture and material properties can be identified using the FGM. Structural analysis of the blade may then be conducted using the finite element method to verify whether the selected material system and fabrication technique meet the design criteria, and fabrication technique may be modified accordingly. This process may be iterated until a final design with an optimal fiber architecture and proven structural behavior is identified. The structural analysis of the composite blade is performed using a general-purpose finite element code [41]. Based on hypothetical blade specifications (Fig. 1.22), a 3-D model is first generated on a computer-aided design (CAD) system; the co-ordinates of the geometry for constructing a finite element mesh are then obtained from this model. Thirty-six 20-node 3-D isoparametric elements are used to model the blade, resulting in a total of 720 nodes. Figure 1.23 shows the finite element mesh established for the turbine blade.

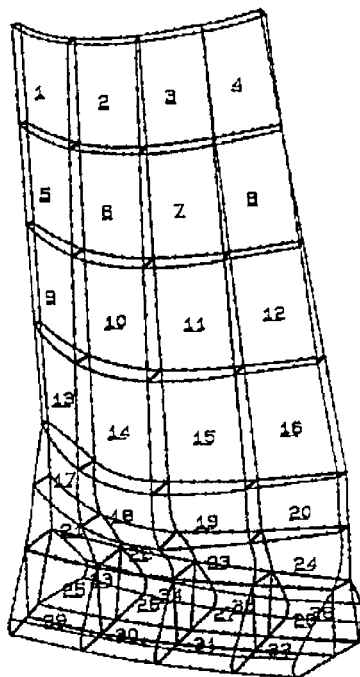
After consideration of several fabrication techniques with different fiber volume fractions, a final design was chosen. The mechanical properties of each fiber architecture are computed from the FGM. The example here is a 3-D braided Nicalon SiC structure in a lithium alumina silicate (LAS III) ceramic matrix. The input material properties and structural parameters for the computation of the system stiffness matrix are presented in Tables 1.3 and 1.4.

The resulting elastic stiffness matrix and the coefficients of thermal expansion for the shank region are given by

$$\begin{pmatrix} 157.6 & 49.4 & 50.2 & 0.4 & 1.2 & 1.2 \\ 49.4 & 156.1 & 52.3 & -0.2 & -0.4 & -0.9 \\ 50.1 & 52.3 & 156.5 & -0.2 & -0.9 & -0.4 \\ 0.4 & -0.2 & -0.2 & 46.7 & -0.6 & -0.6 \\ 1.2 & -0.4 & -0.9 & -0.6 & 43.9 & 0.4 \\ 1.2 & -0.9 & -0.4 & -0.6 & 0.4 & 41.9 \end{pmatrix} \text{ (GPa)}$$



1.22 Low-pressure turbine blade.



1.23 Hypothetical turbine blade showing finite element mesh for Fig. 1.22.

Table 1.3. Materials properties

	Nicalon SiC	LAS III
E_{11} (GPa)	139	181
E_{22} (GPa)	32	181
E_{33} (GPa)	32	181
G_{12} (GPa)	43	60
ρ_{12} (g/cc)	0.20	0.26
α ($10^{-6}/^{\circ}\text{C}$)	3.1	1.6

Table 1.4. Geometric parameters

Braid construction	1×1
Braiding angle θ	± 20
V_f	0.4

with coefficients of thermal expansion

$$\alpha_1 = 1.53 \times 10^{-6}$$

$$\alpha_2 = 1.61 \times 10^{-6}$$

$$\alpha_3 = 1.65 \times 10^{-6}$$

and those of the dovetail region are given by

$$\begin{pmatrix} 154.3 & 51.0 & 51.0 & 1.9 & 2.3 & 2.3 \\ 51.0 & 153.9 & 54.0 & -1.0 & -0.6 & -2.0 \\ 51.0 & 54.0 & 153.9 & -1.0 & -2.0 & -0.6 \\ 1.9 & -1.0 & -1.0 & 49.5 & -1.1 & -1.1 \\ 2.3 & -0.6 & -2.0 & -1.1 & 43.5 & 1.7 \\ 2.3 & -2.0 & -0.6 & -1.0 & 1.7 & 43.5 \end{pmatrix} \text{ (MPa)}$$

with coefficients of thermal expansion

$$\alpha_1 = 1.53 \times 10^{-6}$$

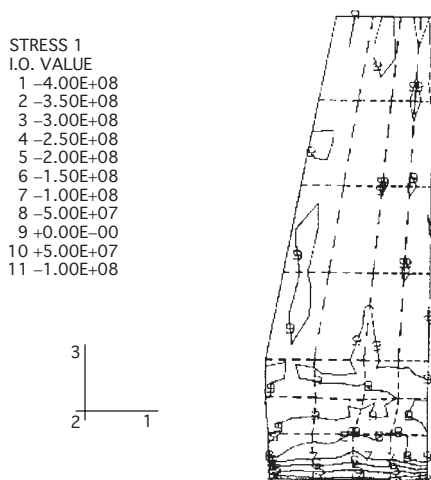
$$\alpha_2 = 1.61 \times 10^{-6}$$

$$\alpha_3 = 1.65 \times 10^{-6}$$

respectively.

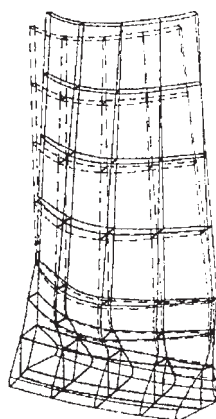
With the stiffness matrix generated according to the input material and geometric properties, one can examine the response of the 3-D composite system to a given thermomechanical condition. For a fixed boundary condition on the bottom surface of the blade, assuming a 1000°C operating temperature and a rotational speed of 4500 rpm, we can evaluate the centrifugal force field as well as the displacement contour on the turbine blade.

Figure 1.24 illustrates a typical stress distribution on the tension surface of the blade for axial (1) stresses. Using this preliminary analysis of this component, the axial stresses in the blade are relatively constant at a value of 50 MPa. In the radial direction, stresses on the shaft of the blade are in the range of 50–80 MPa, with an expected stress concentration at the dovetail region, reaching a predicted level of 170 MPa. Likewise, the shear stress and radial displacement as well as the critical natural frequency of the blade can be determined. To determine the critical natural frequency of the blade, eigen value analysis was carried out. Figure 1.25 shows the second natural mode of the blade. The original mesh is shown with dashed lines, the displaced mesh with solid lines. The frequency associated with this mode is 2.742×10^6 rad/s for mode 2.



1.24 Typical stress distribution for axial stresses.

MAG. FACTOR -- +3.4E-03
SOLID LINES -- DISPLACED MESH
DASHED LINES -- ORIGINAL MESH



1.25 Natural mode of the blade: 2.742×10^6 rad/s (Mode 2).

1.7 Conclusions and future directions

Textile preforms have much to offer to the toughening and to the economic manufacture of the next generation of high-performance structural composites. With a large family of high-performance fibers, linear fiber assemblies, and 2-D and 3-D fiber preforms, a wide range of composite structural performances may be tailored to meet specific requirements. By proper manipulation of the fiber architecture the engineering parameters of the

3-D textile structures can be summarized in terms of their fiber volume fraction–fiber orientation relations. Table 1.5 provides a summary of the range of possible fiber orientation and fiber volume fraction as governed by their respective processing parameters.

The increasing use of 3-D fiber reinforcements for structural toughening of composites poses important technical challenges. The first is the question of conversion of brittle fibrous materials to textile structures, especially for high-temperature and high-stiffness applications. As a rule, the higher the temperature capability of the fiber, the stiffer and more brittle it is. This processing difficulty with brittle fibrous structures calls for an innovative combination of materials systems such as the concept of material and geometric hybridization.

The infiltration or placement of matrix material in a dense 3-D fiber network also creates new challenges. It demands an understanding of the dynamics of the process–structure interaction so that questions such as: ‘What is the optimum pore geometry for pore distribution, bundle size and matrix infiltration?’ can be answered.

As the level of fiber integration increases, the chance of fiber to fiber contact will intensify at the crossover points. This also results in uneven distribution of fiber volume fraction. Guidance will be required to select the fiber preform and matrix placement method best suited to reduce the incidence of localized fiber-rich areas.

Although 3-D fabric reinforcements have been proven to have superior damage resistance and they provide enormous design options in the tailoring of micro- and macro-structures of a composite, the adoption of 3-D reinforcements to commodity structural applications such as in automotive and building constructions has been slow. This can be attributed to the insufficient development of production economics and engineering design capability which must build on a solid engineering database and cost-effective manufacturing technology.

In order to take advantage of the attractive features offered by textile structural composites, there is a need for the development of a sound database and design methodologies which are sensitive to manufacturing technology. An examination of the literature indicated that only a limited number of systematic experimental studies have been carried out on 3-D fabric reinforced composites. A well-established database is needed in order to broaden the usage of fabric reinforced composites for structural applications. The fabric geometry model developed thus far provides a useful framework to integrate fiber architecture design and processing parameters into structural analysis. The precision of strength prediction can be further improved with a better understanding of the failure behavior of 3-D fabric reinforced composites under various loading conditions. Future work in the modeling of fabric reinforced composites requires a better understanding

Table 1.5. Engineering and processing parameters for 3-D textile reinforcements

Preform	Fiber orientation, θ ($^{\circ}$)	V_i	Processing parameter
Linear Assembly Roving yarn	θ , yarn surface helix angle $\theta = 0$ $\theta = 5 \sim 10$	0.6 ~ 0.8 0.7 ~ 0.9	Bundle tension, transverse compression, fiber diameter, number of fibers, twist level
Woven 3-D Woven	θ_f , yarn orientation in fabric plane θ_{cr} , yarn crimp angle $\theta_f = 0/90$, $\theta_c = 30 \sim 60$	-0.6	Fiber packing in yarn, fabric tightness factor, yarn linear density ratios, pitch count, weaving pattern
Non-woven 3-D Orthogonal	θ_x , fiber/yarn orientation along X axis θ_y , fiber/yarn orientation along Y axis θ_z , fiber/yarn orientation along Z axis θ_{xy} , fiber distribution on fabric plane $\theta_{xy} =$ uniform distribution, θ_z θ_x , θ_y , θ_z	0.2 ~ 0.4 0.4 ~ 0.6	2-D non-woven: fiber packing in fabric, fiber distribution 3-D orthogonal: fiber packing in yarn, yarn cross-section, yarn linear density ratios
Knit 3-D MWK	θ_{st} , stitch yarn orientation θ_{ir} , insertion yarn orientation $\theta_s = 30 \sim 60$, $\theta_i = 0/90/\pm 30 \sim 60$	0.3 ~ 0.6	Fiber packing in yarn, fabric tightness factor, yarn linear density ratios, pitch count, stitch pattern
Braid 3-D Braid	θ , braiding angle $\theta = 10 \sim 45$	0.4 ~ 0.6	Fiber packing in yarn, fabric tightness factor, braid diameter, pitch length, braiding pattern, carrier number

of the dynamic interaction among fiber, matrix and fiber architecture. Although the FGM has been used successfully in guiding the selection of materials and textile processing parameters, recent studies have also shown that the improvements in the prediction of shear properties will enhance the accuracy of the fabric geometry model [42].

1.8 References

1. McAllister, L.E. and Lachman, W.L., in *Handbook of Composites*, Vol. 4, Kelly, A. and Mileiko, S.T., eds, North-Holland, Amsterdam, 1983, p. 109.
2. Adsit, N.R., Carnahan, K.R. and Green, J.E., in *Composite Materials: Testing and Design (Second Conference)*, Corten, H.T., ed., ASTM STP 497, Philadelphia, PA, 1972, pp. 107–120.
3. Laurie, R.M., *Polyblends Composites, Appl. Polym. Symp.*, **15**, 103–111, 1970.
4. Schmidt, D.L., *SAMPE J.*, **8**, May/June, p. 9, 1972.
5. Tarnopol'skii, Y.M., Zhigun, I.G. and Polykov, V.A., *Spatially Reinforced Composite Materials*, Moscow Mashinostroyeniye, 1987.
6. Ko, F.K., 'Three-dimensional fabrics for structural composites', in *Textile Structural Composites*, Chou, T.W. and Ko, F.K., eds, Elsevier, Amsterdam, 1989.
7. Ko, F.K., 'Preform fiber architecture for composites', *Ceramic Bull.*, **68**(2), 1989.
8. Scardino, F.L., 'Introduction to textile structures', in *Textile Structural Composites*, Chou, T.W. and Ko, F.K. eds, Elsevier, Covina, CA, 1989.
9. Geoghegan, P.J., 'DuPont ceramics for structural applications – the SEP Noveltex Technology', 3rd Textile Structural Composites Symposium, Philadelphia, PA, 1–2 June, 1988.
10. Fukuta, K., private communication, 1989.
11. Palmer, R., 'Composite preforms by stitching', paper presented at 4th Textile Structural Composites Symposium, Philadelphia, PA, 24–26 July, 1989.
12. Ko, F.K. and Du, G.W., 'Processing of textile preforms', in *Advanced Composites Manufacturing*, Gutowski, T.G., ed., Wiley InterScience, New York, 1998.
13. Dow, R.M., 'New concept for multiple directional fabric formation', in *Proceedings, 21st International SAMPE Technical Conference*, 25–28 September, 1989, pp. 558–569.
14. Stover, E.R., Mark, W.C., Marfowitz, I. and Mueller, W., 'Preparation of an omniweave-reinforced carbon-carbon cylinder as a candidate for evaluation in the advanced heat shield screening program', AFML TR-70283, Drexel University FMRC, March 1979.
15. Herrick, J.W., 'Multidimensional advanced composites for improved impact resistance', paper presented at 10th National SAMPE Technical Conference, 17–19 October, 1977.
16. Pastenbaugh, J., 'Aerospatial technology', paper presented at 3rd Textile Structural Composites Symposium, Philadelphia, PA, 1–2 June, 1988.
17. Bruno, P.S., Keith, D.O. and Vicario, A.A. Jr, 'Automatically woven three dimensional composite structures', *SAMPE Quarterly*, **17**(4), 10–16, 1986.
18. O'Shea, J., 'Autoweave: a unique automated 3-D weaving technology', paper presented at 3rd Textile Structural Composites Symposium, Philadelphia, PA, 1–2 June, 1988.

19. Fukuta, K. and Aoki, E., '3-D fabrics for structural composites', paper presented at 15th Textile Research Symposium, Philadelphia, PA, September 1986.
20. Fukuta, K., Aoki, E., Onooka, R. and Magatsuka, Y., 'Application of latticed structural composite materials with three dimensional fabrics to artificial bones', *Bull. Res. Inst. Polymers Textiles*, **131**, 159, 1982.
21. Williams, D.J., 'New knitting methods offer continuous structures', *Adv. Composites Eng.*, **Summer**, 12–13, 1978.
22. Hickman, G.T. and Williams, D.J., '3-D knitted preforms for structural reactive injection molding (SRIM)', in *Proceedings of the Fourth Annual Conference on Advanced Composites*, ASM International, 1988, pp. 367–370.
23. Ko, F.K. and Kutz, J., 'Multiaxial warp knit for advanced composites', in *Proceedings of the Fourth Annual Conference on Advanced Composites*, ASM International, 1988, pp. 377–384.
24. Ko, F.K., Pastore, C.M., Yang, J.M. and Chou, T.W., 'Structure and properties of multidirectional warp knit fabric reinforced composites', in *Composites '86: Recent Advances in Japan and the United States*, Kawata, K., Umekawa, S. and Kobayashi, A., eds, Proceedings, Japan-US CCM-III, Tokyo, 1986, pp. 21–28.
25. ITA Research Information Bulletin, University of Aachen, 1998.
26. Du, G.W. and Ko, F.K., 'Analysis of multiaxial warp knitted preforms for composite reinforcement', paper presented at Proceedings of Textile Composites in Building Construction Second International Symposium, Lyon, France, 23–25 June, 1992.
27. Ko, F.K., 'Three-dimensional fabrics for structural composites', in *Textile Structural Composites*, Chou, T.W. and Ko, F.K., eds, Elsevier, Tokyo, 1989.
28. Brown, R.T. and Ashton, C.H., 'Automation of 3-D braiding machines', paper presented at 4th Textile Structural Composites Symposium, 24–26 July, 1989.
29. Popper, P. and McConnell, R., 'A new 3-D braid for integrated parts manufacturing and improved delamination resistance – the 2-step method', *32nd International SAMPE Symposium and Exhibition*, 1987, pp. 92–102.
30. Du, G.W. and Ko, F.K., 'Geometric modeling of 3-D braided preforms for composites', paper presented at 5th Textile Structural Composites Symposium, Drexel University, Philadelphia, PA, 4–6 December, 1991.
31. Ko, F.K., Chu, J.N. and Hua, C.T., 'Damage tolerance of composites: 3-D braided commingled PEEK/carbon', *J. Appl. Polymer Sci.: Appl. Polymer Symp.*, **47**, John Wiley, New York, 1991.
32. Liao, D., 'Elastic behavior of 3-D braided composites under compressive loading', PhD thesis, Drexel University, June, 1990.
33. Lei, C.S.C. and Ko, F.K., 'Mechanical behavior of 3-D braided hybrid MMC', paper presented at ICCM-8, 12–16 July, 1991.
34. Ko *et al.*, 'Toughening of SiC/LASIII ceramic composites by hybrid 3-D fiber architecture', paper presented at ICCM-7, 1989.
35. Dow, N.F. and Ramnath, V., 'Analysis of woven fabrics for reinforced composite materials', NASA Contract Report 178275, 1987.
36. Chou, T.W. and Yang, J.M., 'Structure–performance maps of polymeric metal and ceramic matrix composites', *Metallurgical Transaction A*, **17A**, 1547–1559, 1986.
37. Ko, F.K., Pastore, C.M., Lei, C. and Whyte, D.W., 'A fabric geometry model for 3-D braid reinforced FP/Al-Li composites', paper presented at 'Competitive

- Advancements in Metals/Metals Processing', SAMPE Meeting, Cherry, NJ, 18–20 August, 1987.
38. Cox, B. and Flanagan, G., *Handbook of Analytical Methods for Textile Composites*, Version 1.0, Rockwell Science Center, Thousand Oaks, CA, January, 1996.
 39. Pastore, C.M. and Ko, F.K., 'Modelling of textile structural composites: part 1: a processing science model for three-dimensional braid', *J. Textile Inst.*, **81**(4), 480–90, 1990.
 40. Tan, T.M., Pastore, C.M. and Ko, F.K., *Engineering Design of Tough Ceramic Matrix Composites for Turbine Components*, ASME, Toronto, 1989.
 41. *ABAQUS Manual*, Hibbit, Carlson and Sorensen, Inc, 1982.
 42. VanDeurzen, P., 'Structure–performance modeling of two-dimensional woven fabric composites', PhD Thesis, Katholieke Universiteit Leuven, Belgium, 1998.

